Is low-temperature fission-track annealing in apatite a thermally controlled process?

M. T. Tamer[1], and R. A. Ketcham[1]

[1]Department of Geological Sciences, Jackson School of Geoscience, University of Texas, Austin, TX, USA.

Corresponding author: Richard Ketcham (ketcham@jsg.utexas.edu)

Key Points:

- We document apatite fission-track annealing at earth-surface conditions in the seconds to decades after track formation.
- Empirical annealing equations encompass most low- and high-temperature experimental data, indicating that the same processes control both.
- There is evidence of a distinct annealing process operating during the seconds after induced track formation.

Abstract

We report a new series of experiments to explore the phenomenon of low-temperature annealing of fission tracks in apatite that feature a number of improvements over previous work. Grain mounts were pre-irradiated ^{252}Cf to increase confined track detection and allow briefer thermal neutron irradiation. We co-irradiated and etched four apatite varieties (Durango, Fish Canyon, Renfrew, Tioga) over five time steps equally spaced from 3.66 to 15 ln(s). A length standard was co-etched with all experiments to ensure that subtle differences are within detection limits. Finally, we used a standard etching protocol, allowing the data to be co-modeled with extensive high-temperature data sets and recent analyses of induced tracks that underwent ambient-temperature annealing over year-to-decade time scales. Ambient-temperature annealing occurs at two different rates, with faster annealing at early stages that decreases to a slower rate that converges with empirical fanning linear or curvilinear models. The nature of this decrease varies among the apatite species examined, but no patterns could be determined. The fitted models make geological time-scale predictions consistent with those based on high-temperature data only, and also make predictions consistent with reasonable inferred low-temperature histories for all four apatite varieties. The empirical fanning curvilinear equation encompasses low-temperature annealing at month-to-decade time scales, but low-temperature annealing at shorter time scales may occur by a distinct mechanism. We consider but rule out annealing by radiation from short-lived activated isotopes. We also reconsider the notion of the initial track length, and the appropriate length for normalizing confined track length measurements.

Plain Language Summary

We present a new series of experiments to study the extent to which the radiation damage from fission decay of uranium in the mineral apatite is annealed (healed) at room temperature. We combine data obtained by etching fission tracks seconds after being generated in a nuclear reactor with tracks etched minutes, hours, days, months, years, and even decades after generation, and find that detectable annealing occurs over these time spans. We combine these data with previous experiments conducted at high temperatures to see whether the model equations currently used to describe high-temperature annealing can encompass the low-temperature data, which would support the idea that the same atomic-scale processes control both. We find that most of our low-temperature data are consistent with the high-temperature data and model equations, with the exception of earliest-stage experiments that show faster-than-expected annealing, possibly caused by a different process. We consider but reject a possible annealing effect from secondary radiation. These data make it clear that a truly "unannealed" track length is unmeasurable, which in turn requires that we reconsider how we normalize measurements of annealed lengths. Our measurements also allow us to more confidently characterize fission-track annealing at earth-surface conditions over geological time scales.

1 Introduction

Fission decay results in charged particles as disintegration products, whose interactions with surrounding crystalline material result in damage trails called fission tracks (Silk & Barnes, 1959), which can be hosted in extra-terrestrial (Fleischer et al., 1967) and terrestrial minerals (Price & Walker, 1963). With suitable etching procedures these tracks become observable under optical microscopes (Fleischer et al., 1965b). Fission tracks can be generated by spontaneous fission of ^{238}U and accumulate over geological time, or induced by thermal neutron irradiation of ^{235}U in nuclear reactors (Meitner & Frisch, 1939). Depending on the host material and time and

temperature conditions, the displaced atoms undergo reconstruction (Fleischer et al., 1965a), resulting in progressive and eventually complete fading of fission tracks, which is called annealing (Fleischer & Price, 1964). Progressive annealing allows fission tracks to carry information on the time and temperature conditions experienced by the host material from the moment of generation until etching, which can be accessed using fission track lengths. Apatite is one of the most investigated minerals for fission track thermochronology (Naeser, 1967; Wagner, 1968) due to its abundance in various rocks and geological environments, ability to concentrate sufficient amounts of U, and its straightforward etching procedure (Donelick et al., 2005).

Spontaneous tracks in apatite are shorter than freshly generated induced tracks in all cases, even in samples with no significant geological heating (Gleadow et al., 1986; Green, 1988; Jonckheere, 2003; Spiegel et al., 2007; Vrolijk et al., 1992), suggesting that annealing occurs at ambient Earth surface temperatures. Length reduction at ambient temperatures has also been documented in induced tracks at laboratory time scales from minutes to years after irradiation (Donelick et al., 1990; Tamer et al., 2019). It remains unclear, however, whether this ambient-temperature annealing reflects the same atomic scale processes that control annealing at elevated temperatures, and by extension whether it can or should be characterized by the same governing equations.

1.1 Ambient-temperature annealing at laboratory time scales

Evidence of track annealing at low temperatures and short time scales was reported by Donelick et al. (1990) for various apatites with different chemical compositions. Two groups of pre-annealed apatite mounts were irradiated at two different reactors at different thermal neutron fluences (ϕ=~1*10^{15} and ~8*10^{15} n/cm^2) for times as brief as 37 s, and etched after waiting periods ranging from 3 minutes to 125 days, mainly grouped at ~6 and ~15 ln(s), or about 10 minutes and 38 days, respectively. Mean confined fission-track lengths decreased measurably over this period. The Donelick et al. (1990) result is consistent with spontaneous confined track lengths being shorter than induced tracks in Fish Canyon Tuff (28±2 Ma) apatite and Durango apatite (31±3 Ma), which have been assumed to have not experienced significant heating above ambient earth-surface temperatures since emplacement (Gleadow et al., 1986; McDowell et al., 2005). A re-analysis of the Donelick et al. (1990) data for Tioga apatite, combined with higher-temperature experiments by Donelick (1991), indicates that this low-temperature annealing is well described by the empirical equations used to describe fission-track annealing (e.g., Donelick et al., 1999; Ketcham et al., 2007b; Laslett et al., 1987), suggesting that it may be controlled by the same process. However, these data sets were generated with an etching protocol that is no longer used, and the high-temperature experiments may have suffered from temperature calibration issues (Carlson et al., 1999), making this result suggestive but not definitive.

1.2 Ambient-temperature annealing at decadal time scales

Previous experiments (Belton, 2006; Tamer et al., 2019) have documented low-temperature annealing at decadal time scales. Annealing studies on induced tracks in apatite have been conducted since the 1970's, and materials from those irradiations have been experiencing ambient temperatures for up to 50 years. A recent study (Tamer et al., 2019) used such material to document a ~0.2 μm decrease in mean track length over a time range of ~2-44 years in four different apatite species; additional analyses reported in this study further document these year-to-decadal annealing trends.

1.3 This study

To increase our understanding of ambient-temperature length reduction, we designed a study building and improving upon Donelick et al. (1990) in several ways. The first is to implant ^{252}Cf tracks into the polished surface of pre-annealed apatite grain mounts prior to neutron irradiation and etching, to increase the number of induced confined tracks etched (Donelick & Miller, 1991). This measure allows us to decrease the thermal neutron irradiation time and commence experiments as quickly after the onset of track formation as possible. The second is to irradiate more (five) aliquots to obtain more observation points to document short-term annealing, with regular sampling across a larger time range. The third improvement is to etch c-axis-parallel cut Durango apatite crystals containing fossil tracks along with each irradiated mount, to provide an additional rigorous control on the etching quality and consistency for each experiment. The fourth improvement is studying a wider kinetic range of apatite species and applying a standard etching protocol (5.5 M HNO_3, 20s, 21°C) that allows us to link results to more extensive high-temperature annealing data sets (Carlson et al., 1999).

We also assembled data documenting low-temperature annealing at decadal time scales, combining new measurements on the same apatites irradiated at various times in the past with literature values acquired using the identical etching procedure (Carlson et al., 1999; Tamer et al., 2019).

Finally, we combine high- and low-temperature annealing data to fit new annealing models for various apatites, and compare them with previous fits based only on high-temperature experiments. This allows us to both examine whether the low-temperature data are consistent with the annealing behavior implied by the high-temperature results, and the extent to which the concept of "unannealed" track length used in previous studies requires reconsideration or modification (cf. Laslett & Galbraith, 1996).

2 Materials and Methods

2.1 Samples

Table 1 lists sample details. We selected apatite species for this study using several criteria. Availability of material from earlier irradiations was necessary to allow co-investigation of decadal ambient temperature annealing. We also wanted apatites that had been previously studied using high-T annealing experiments. Another advantage was for the natural samples to have a well-studied, distinct thermal history of rapid cooling followed by solely ambient temperature annealing over geological time scales, allowing us to monitor any new model predictions based on corresponding spontaneous track data. Durango (DR) and Fish Canyon Tuff (FC) apatite fit all three criteria, while Renfrew (RN) and Tioga (TI) apatite satisfy the first two, but have not previously had thermal histories estimated. In all, 33 aliquots from these four apatite species from two different fission-track laboratories (University of Texas at Austin and University of Melbourne) were measured, of which 20 were irradiated for this study, nine were irradiated previously, and four samples had fossil tracks. Additionally, five DR apatite samples with spontaneous tracks were used as etching quality monitors.

Table 1. *Apatite specimens used in this study*.

Apatite	Locality	This study	Previous irradiations				Samples with fossil tracks	Composition (apfu)[1]		
		Apatite source[2]	Apatite source[2]	Irradiation location[2]	Irradiation date	Track age (ln(s))	Apatite source[2]	F	Cl	OH
DR	Cerro de Mercado, Durango, Mexico	UT	UT	UT	5/12/2014	18.32[4]	UT	1.80	0.13	0.07
			UT	TAMU	2/1/1992[3]	20.51				
			UM	UM	3/8/1990	20.56[4]				
			UM	UM	2/20/1985	20.74[4]				
FC	Fish Canyon Tuff, San Juan Mountains, Colorado, U.S.A	UT	UT	UT	5/12/2014	18.49	UT	1.12	0.23	0.65
RN	Renfrew Rensselaer Ontario, Canada	UM	UT	TAMU	2/1/1992[3]	20.51	UM	1.81	0.01	0.18
			UM	UM	3/8/1990	20.56[4]				
			UM	UM	2/20/1985	20.74[4]				
TI	Tioga ash bed near Old Port, Pennsylvania, U.S.A	UT	UT	TAMU	2/1/1992[3]	20.51	UT	0.87	0.17	0.96

[1] Composition data from Carlson et al. (1999); stoichiometry calculations from Ketcham (2015). [2] Location codes: TAMU=Texas A&M University; UM=University of Melbourne; UT=University of Texas at Austin. [3] Date approximate within one month. [4] Track measurement data from Tamer et al. (2019).

2.2 Laboratory time scale annealing experiments

Apatites to be irradiated were first annealed at 450°C for 48h to erase all spontaneous tracks. Five epoxy grain mounts were prepared for irradiation, each containing pre-annealed aliquots of all four apatites. The grains from different apatite species were placed in distinct parts of the mount and kept isolated from each other during preparation. The five DR apatite monitor mounts were prepared separately. After polishing to reveal internal grain surfaces, both the experimental and monitor mounts were ^{252}Cf-irradiated (~1×10^{15} tracks/cm^2).

The experimental mounts were then placed in a sealed plastic container and irradiated at the University of Texas Nuclear Engineering Teaching Lab (NETL) TRIGA Mark II nuclear research reactor. A pneumatic system allowed us to load samples from a fume hood, transfer them to the reactor, and quickly retrieve them after irradiation. The samples were irradiated for 20 s with a thermal neutron fluence of ~$8*10^{15}$ n/cm^2, and returned to the fume hood 10 s after irradiation. Upon arrival, the samples were extracted from the container, and within ~4 s one of the irradiated mounts was etched together with one of the DR monitor mounts. The sample and monitor were etched with 5.5 M HNO_3 for 20 seconds at 21 °C and immersed in water immediately afterwards. The other irradiated mounts were etched together with monitors after longer intervals, as listed in Table 2.

Table 2. *Etching times and monitor measurements*.

Exp	Etching time after irradiation			Co-etched monitor data (μm)					
	s	ln(s)	Various	N	l_m	σ_{lm}	N	D_{par}	σ_{Dpar}
1	39	3.66	39 seconds	81	14.55 (07)	0.67	41	1.87 (02)	0.11
2	1098	7.00	18.3 minutes	64	14.41 (08)	0.65	35	1.85 (02)	0.10
3	21996	10.00	6.11 hours	60	14.59 (10)	0.79	40	1.82 (02)	0.11
4	162432	12.00	1.88 days	45	14.69 (09)	0.61	48	1.80 (01)	0.09
5	3269017	15.00	37.8 days	47	14.44 (09)	0.60	41	1.81 (01)	0.09

Special considerations apply for reporting the annealing interval for the first experiment. We assume that a fission track anneals from the moment it is generated until it is etched to its tips. During irradiation tracks are continuously generated, and thus some tracks experienced 20s of reactor-ambient temperatures while others were forming. Similar considerations apply for the etching time, which is different for every confined track depending on when the impinging track creating the etchant pathway enlarges sufficiently to intersect it. The total duration for the first experiment was 54 seconds: 20 seconds for irradiation, 10 seconds for sample transfer, 4 seconds for sample extraction from the sealed container and 20 seconds of etching. We estimate the mean formation time as 10 seconds after the irradiation began, and mean etching completion to be 15 seconds after the etch began, based on step etching experiments, resulting in an average ambient temperature annealing time for the first experiment of 39 seconds (3.66 ln(s)).

2.3 Decadal time scale annealing experiments

The annealing study by Carlson et al. (1999) included the four apatite species used in this study. Unused irradiated apatites from the Carlson et al. (1999) study have

experienced ~27 years of ambient-temperature annealing. We prepared additional mounts of this material for each apatite species for induced track length measurements to evaluate annealing over this time.

2.4 Measurements

All fission track length and etch figure length (D_{par}) measurements were carried out at the Fission Track Laboratory at the Jackson School of Geosciences at the University of Texas at Austin. The mounts were scanned to find the grains parallel to crystallographic c-axis, and images of confined fission tracks were captured with a Zeiss M2m Axio Imager microscope using TrackWorks v3 software. Length measurements on the images used FastTracks v3 software.

3 Data analysis methods

3.1 **C**-axis projection

To help account for anisotropy, we first determined the most appropriate **c**-axis projection model for our measurements. The inter-laboratory study by Ketcham et al. (2015, Fig. 6) compared fitted ellipse intercepts (l_c and l_a) from measurements of four induced confined track length standards for each participant with trends from two major data sets acquired with different etching protocols: Carlson et al. (1999) with 5.5 M HNO_3 20s 21°C, and Barbarand et al. (2003), with 5.0 M HNO_3 20s 20°C. They found that the l_c vs. l_a slope was not dependent on etching, as previously supposed, but on analyst-specific factors that have not yet been identified. A fitted regression line of our measurements of the same standards exhibits a trend more similar to the Barbarand et al (2003) result, and so we use the 5.0M projection model from Ketcham et al. (2007a) to calculate individual and mean **c**-axis projected lengths for our data. We did not calculate projected lengths for the Donelick et al. (1990) data due to their distinct etching protocol (5.0 M HNO_3 25s 23°C), and instead use the individually-fitted ellipse values they reported.

Because of the low annealing level of many of our samples, some of the very long lengths encountered (>18 µm) were beyond the range encompassed in the **c**-axis projection model, causing their projected lengths to be shorter than the actual measured length. For these tracks the projected length was assumed to be equal to their actual, non-projected length.

3.2 Fitting annealing models

3.2.1 Background

All modern interpretation and modeling of fission-track data rests on the assumption that spontaneous tracks annealing over geological time scales and conditions can be represented adequately by induced tracks annealing at laboratory time scales and conditions. A corollary assumption is that the annealing mechanism is the same in both situations. Yet another assumption is that the empirical models currently used to fit fission-track data reflect the underlying physical mechanism(s) sufficiently well to make such extrapolations with reasonable accuracy.

Our new data test these assumptions in a number of ways. Because they include annealing at lower temperatures over time scales both shorter and longer than any included in previous annealing data sets or models, they significantly extend the range of

conditions that need to be encompassed. Because this extended thermal regime directly overlaps relevant geological conditions, our data relate more directly to the conditions experienced by and processes operating within geological samples. Furthermore, insofar as most annealing models are based on lengths normalized to an "unannealed" state, progressive annealing at surface temperatures raises the question of what this state is, and thus what the normalizing value should be, or mean. Most previous studies have assumed that tracks etched some number of months after irradiation can be considered unannealed for modeling purposes without significant penalty (e.g., Crowley et al., 1991; Ketcham et al., 2007b; Ketcham et al., 1999; Laslett et al., 1987).

This last point has additional practical implications. Measurements of mean initial track length (l_0) are typically executed 2-18 months after irradiation, after some low-temperature annealing may have taken place. Measured values vary among apatite varieties by over 1 µm (Carlson et al., 1999), enough to affect thermal history interpretation and inversion. Laslett and Galbraith (1996) explored making the normalizing value a fitted parameter (μ_{max}) in their reconsideration of data from Crowley et al. (1991), but their approach gave the non-intuitive result that two apatite varieties with measured l_0 values less than 0.1 µm apart had μ_{max} values 2.25 µm apart. Ketcham et al. (1999, Appendix B) conducted a similar exercise and got a less severe but still unsatisfying result, with fitted normalizing values from 4-14% longer than measured ones for various apatites, and no evident way to determine how large the correction should be when analyzing an unknown apatite. Ketcham et al. (2007b) also experimented with such a correction when combining the data sets of Carlson et al. (1999) and Barbarand et al. (2003) into a single annealing model, and rejected the result when identical apatites measured by different analysts gave very different corrections.

Given these considerations, we raise three questions to focus the present study. (1) Is ambient-temperature annealing over seconds to decades predicted by or encompassed in current annealing models? (2) Is there a reliable way to measure or estimate the true unannealed mean track length? (3) How should the normalizing value for track lengths be defined and determined?

3.2.2 Annealing model equations

The general form of the empirical annealing model is (Ketcham et al., 1999):

$$g(l; l_0, \alpha, \beta) = f(t, T; C_i) \tag{1}$$

where g transforms the lengths according to the measured initial track length (l_0), and up to two fitted parameters α and β; and f is a function of time (t), temperature (T), and a series of fitted parameters (C_i). The model fits a normalized or "reduced" track length r, defined as l/l_0, which is assumed to have a maximum value of one. Because we are including data from different sources (Carlson et al., 1999), we use different measured l_0 values for each analyst.

The general form of g stems from the Box-Cox "super-model" used by Laslett et al. (1987),

$$g = \left\{\left[\left(1 - r^{\beta}\right)/\beta\right]^{\alpha} - 1\right\}/\alpha \tag{2}$$

Certain values of α and β simplify the equation. Following from the final recommended model of Ketcham et al. (2007b), we use β = -1, and simplify further by folding the final terms into the C_i parameters for f.

To account for the possibility of a longer "true" initial track length, and to permit inclusion of short-time-scale measurements while still using a 2-12-month post-irradiation measurement for l_0, we include an adjustment factor τ to modify l_0, resulting in:

$$g = \left(\frac{\tau}{r} - 1\right)^{\alpha} \quad (3)$$

The relation between τ, l_0, and μ_{max} is $\mu_{max} = \tau\, l_0$. To ensure $\tau/r > 1$, the minimum value for τ is 1.0001 l_{max}/l_0, where l_{max} is the maximum mean length measured (in each case here, the value at 3.66 ln(s)), and it is allowed to vary up to a maximum of 1.2, meaning the adjusted initial length is allowed to be up to 20% longer than the value measured months after irradiation.

We investigate two empirical models proposed previously to describe the annealing of fission tracks. The fanning Arrhenius model (FA) (Laslett et al., 1987),

$$f = C_0 + C_1 \left[\frac{\ln(t) - C_2}{(1/T) - C_3}\right] \quad (4)$$

defines a single fanning point in Arrhenius space and fits a set of linear iso-annealing contours emanating from that point. The fanning curvilinear model (FC) (Crowley et al., 1991; Ketcham et al., 1999),

$$f = C_0 + C_1 \left[\frac{\ln(t) - C_2}{\ln(1/T) - C_3}\right] \quad (5)$$

is similar but fits fanning contours that are linear in log-log space but slightly curved in Arrhenius space.

In keeping with previous work, we explore functions fit to both mean length and mean **c**-axis projected length data. Although we also calculated individual ellipse fits for all experiments, the results showed excess scatter, due largely to the sparsity of low-angle tracks (Donelick et al., 1999; Ketcham, 2003). We fitted the model parameters using chi-squared minimization as described by Ketcham et al. (1999, Appendix A). Results are accompanied by a series of index temperatures helpful for inferring geological time-scale predictions (Ketcham et al., 1999). The closure temperature (T_C) is the temperature of the measured age (Dodson 1973, 1986) assuming linear cooling from high temperature. The fading temperature (T_F) is the down-hole temperature where fission track density drops to zero after isothermal holding of a given duration (Gleadow & Duddy, 1981; Naeser et al., 1981). The total annealing temperature (T_A) defines where a fission-track population will totally anneal with linear heating, or equivalently the highest temperature experienced by any surviving fission track during cooling (Issler, 1996; Ketcham et al., 1999). T_C and T_A are given for various cooling rates (in °C/m.y.); and T_F varies with the duration of the isothermal episode (given in m.y).

4 Results

4.1 Durango spontaneous track monitor samples

The mean track length and etch figure measurements of the monitor samples are listed in Table 2, and shown in Figure 1. The monitor data show no systematic change, and variation is minor, with a range of <0.3 µm for mean track length and <0.1 µm for mean D_{par} value, verifying that etching procedures were consistent across the experiment,

and that the subtle length changes reported below are within the resolution limit of this study.

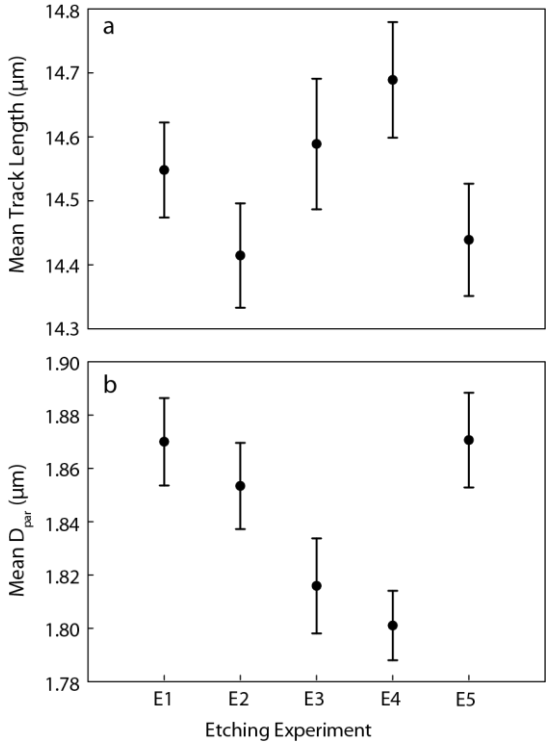

Figure 1: Mean track length and D_{par} measurements of Durango apatites co-etched with each etching experiment.

4.2 Ambient-temperature annealing

Summaries of non-projected and **c**-axis projected track length measurements, as well as fitted ellipse axes, are listed in Table 3. The mean non-projected and projected track lengths from this study, combined with data from Tamer et al. (2019), Donelick et al. (1990), and Carlson et al. (1999) are shown as points with error bars in Figure 2. Also shown for reference are spontaneous track length measurements for each apatite, although they are non-equivalent to the experimental induced-track data in at least two ways. First, the individual tracks are of varying age, having formed continuously throughout the samples' respective geological histories; for this reason, we plot each point at half the sample age, to represent the mean age of the spontaneous tracks. Second, their annealing temperatures are unknown, although the assumption that the Durango and Fish Canyon localities remained near the Earth surface has independent support (Gleadow et al., 2015; McDowell et al., 2005).

Table 3. *Non-projected, modeled c-axis projected, and ellipse fits to confined fission-track lengths.*

Apatite	Track age (ln(s))	*N*	l_m (µm)	σ_m	$l_{c,mod}$ (µm)	$\sigma_{lc,mod}$	$l_{c,fit}$ (µm)	$l_{a,fit}$ (µm)	$\sigma_{ellipse}$
DR	3.66	26	16.58 (11)	0.54	16.72 (09)	0.44	16.71 (51)	16.52 (25)	0.54
	7.00	29	16.35 (10)	0.54	16.52 (08)	0.43	16.24 (32)	16.40 (19)	0.54
	10.00	33	16.32 (11)	0.61	16.50 (09)	0.51	16.55 (27)	16.15 (22)	0.60
	12.00	33	16.25 (09)	0.49	16.46 (06)	0.36	16.47 (38)	16.16 (19)	0.49
	15.00	28	16.09 (09)	0.45	16.35 (07)	0.35	16.23 (48)	16.04 (19)	0.45
	18.32[1,3]	169	16.06 (05)	0.68	16.32 (04)	0.51	16.31 (18)	15.96 (09)	0.67
	20.51	177	15.92 (05)	0.70	16.21 (04)	0.52	16.29 (16)	15.77 (08)	0.69
	20.56[1]	158	15.90 (06)	0.74	16.20 (04)	0.56	16.02 (17)	15.86 (09)	0.74
	20.74[1]	159	15.84 (06)	0.72	16.15 (04)	0.53	16.28 (17)	15.65 (09)	0.70
	34.53[2]	87	14.43 (08)	0.78	15.08 (06)	0.54	15.21 (20)	14.06 (12)	0.69
FC	3.66	28	17.03 (14)	0.73	17.12 (12)	0.66	17.33 (36)	16.99 (22)	0.72
	7.00	45	16.69 (08)	0.54	16.79 (07)	0.46	16.51 (30)	16.78 (19)	0.54
	10.00	26	16.54 (12)	0.63	16.67 (10)	0.53	16.66 (39)	16.47 (25)	0.63
	12.00	32	16.45 (12)	0.69	16.63 (10)	0.56	16.70 (43)	16.36 (20)	0.69
	15.00	23	16.35 (13)	0.64	16.52 (12)	0.56	16.14 (36)	16.50 (28)	0.64
	18.49[3]	57	16.26 (08)	0.62	16.47 (06)	0.47	16.78 (29)	16.02 (15)	0.59
	34.43[2]	109	14.93 (07)	0.71	15.45 (05)	0.56	15.09 (20)	14.86 (11)	0.71
RN	3.66	9	17.13 (23)	0.69	17.19 (21)	0.64	17.57 (56)	16.92 (34)	0.65
	7.00	10	16.95 (16)	0.50	17.01 (14)	0.44	16.10 (73)	17.04 (35)	0.49
	10.00	9	16.87 (16)	0.55	16.93 (16)	0.49	16.56 (50)	17.09 (41)	0.52
	12.00	14	16.43 (14)	0.54	16.59 (11)	0.43	15.84 (59)	16.68 (32)	0.50
	15.00[3]	18	16.11 (12)	0.51	16.32 (10)	0.44	15.83 (43)	16.27 (28)	0.49
	20.51	151	15.96 (05)	0.64	16.27 (04)	0.46	16.59 (26)	15.80 (08)	0.62
	20.56[1]	164	15.78 (06)	0.71	16.09 (04)	0.54	15.95 (16)	15.66 (09)	0.71
	20.74[1]	170	15.64 (06)	0.73	15.97 (04)	0.55	15.82 (14)	15.54 (09)	0.72
	36.30[2]	106	13.70 (13)	1.39	14.52 (10)	1.04	14.35 (19)	13.39 (11)	1.36
TI	3.66	72	17.03 (08)	0.65	17.14 (07)	0.56	17.33 (22)	16.88 (13)	0.64
	7.00	66	16.78 (07)	0.60	16.87 (06)	0.52	16.82 (22)	16.76 (13)	0.60
	10.00	59	16.56 (07)	0.50	16.70 (05)	0.41	16.41 (30)	16.62 (15)	0.50
	12.00	50	16.33 (08)	0.58	16.51 (06)	0.45	16.43 (31)	16.27 (18)	0.58
	15.00	69	16.24 (07)	0.58	16.45 (05)	0.45	16.37 (27)	16.19 (14)	0.58
	20.51[3]	148	16.22 (06)	0.68	16.46 (04)	0.50	16.92 (21)	16.00 (08)	0.64
	37.05[2]	113	14.03 (10)	1.10	14.80(08)	0.83	14.45 (20)	13.87 (10)	1.09

[1]Measurement data from Tamer et al. (2019). [2]Apatites with spontaneous tracks; AFT ages for DR, FC, RN; monazite U/Pb for TI. [3]Experiment used for l_0.

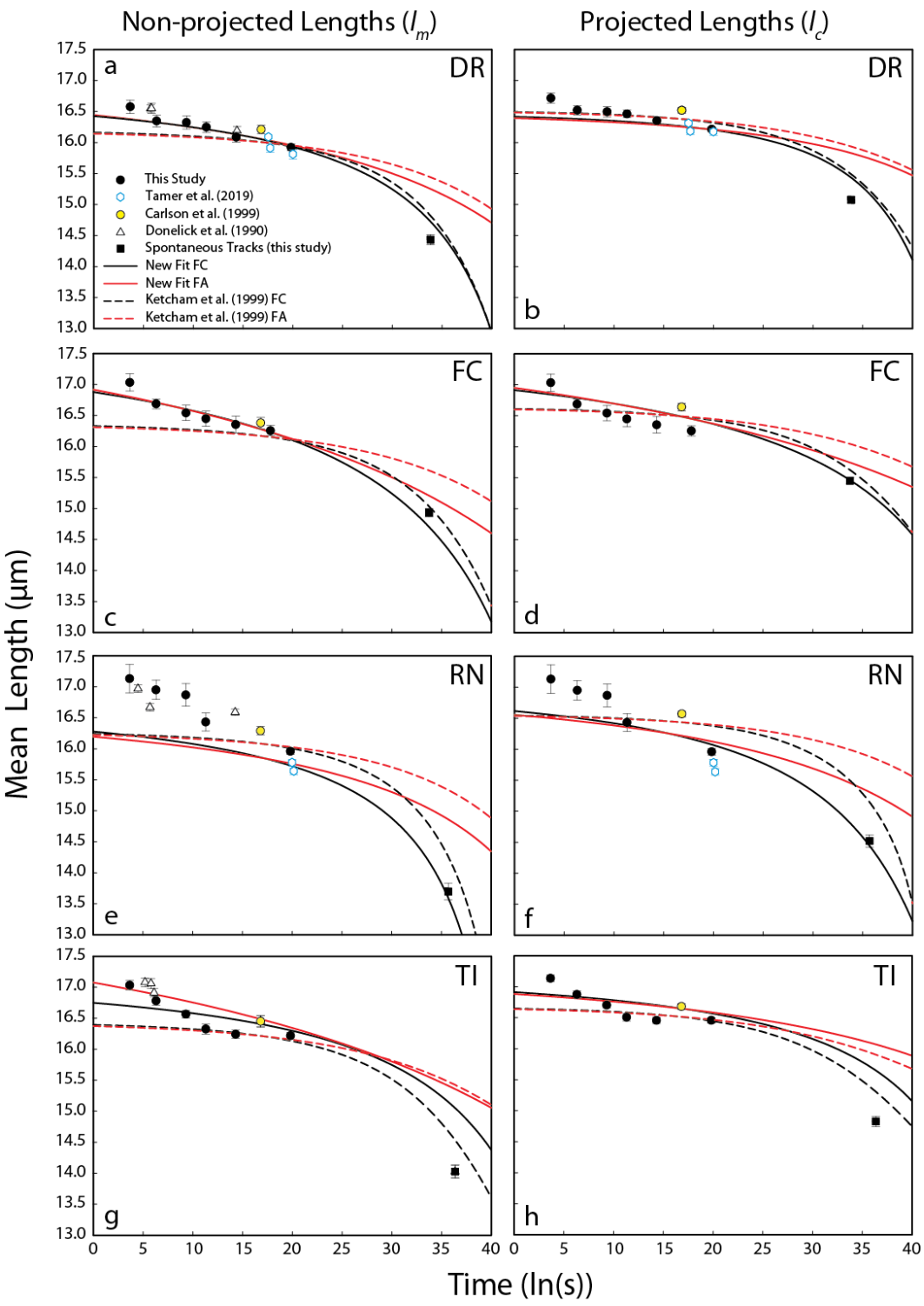

Figure 2: Evolution of mean non-projected (a,c,e,g) and **c**-axis projected (b,d,f,h) track length with time at ambient temperatures, with new (solid) and previous (dashed) model fits for four apatites from four data sets. FA = fanning Arrhenius, FC = fanning curvilinear.

In all four apatites, for both projected and non-projected lengths, there is a continuous decrease in mean track length with time at ambient temperatures. Broadly speaking, all four show a pattern of initial fast annealing that slows down as time scales extend from seconds to years. However, the timing and severity of this deceleration varies among apatites. DR and FC annealing rates decelerate after the first experiment, while TI annealing appears to decelerate after the fourth. RN apatite has an unusual pattern of apparent initial slow annealing followed by acceleration and then deceleration, though the signal is unclear due to very low track numbers stemming from its low U content. However, the longer-time-scale RN data (ln(s)=15-20) imply a continuing fast annealing trend not evident for the other apatites.

Our measurements are broadly consistent with prior work by Donelick et al. (1990). Data for DR are extremely congruent, and the RN pattern is similar in its irregularity, especially considering the Carlson et al. (1999) l_0 value by the same analyst (R. Donelick), though the earlier measurement used a different etching protocol. Perhaps the largest difference is that the Donelick et al. (1990) and Carlson et al. (1999) data for Tioga apatite seem to define a consistent trend, albeit one defined by two clusters of closely spaced points, whereas our data suggest two stages with differing annealing rates.

Also shown in Figure 2 as dashed lines are the predicted lengths at 23°C for annealing models by Ketcham et al. (1999). The models shown for DR and RN are the versions fitted to only the data for those respective apatites (Ketcham et al., 1999, Table 3). Because Carlson et al. (1999) only conducted 13 experiments for TI and FC, for those apatites we plotted the predictions of the multi-apatite models (Ketcham et al., 1999, Table 5), using the apatites' respective apatite-apatite fitting parameters r_{mr0} and κ (Ketcham et al., 1999, Table 4). In each case, because the l_0 measured after ~1 year of ambient annealing was used for the previous models, the maximum possible model track length was substantially shorter than the shorter-time experiments reported here, precluding them from reproducing our new data. It should be noted, however, that the Ketcham et al. (1999) equations do predict some annealing over month-to-decade time scales, which is why they under-predict the plotted Carlson et al. (1999) l_0 points (yellow circles in Figure 2), instead asymptotically approaching these values as log time approaches -∞. Also noteworthy is that the Carlson et al. (1999) fanning curvilinear curves for DR and FC come close to the spontaneous track measurements, illustrating how those models broadly agree with the low-temperature annealing benchmarks proposed by Ketcham et al. (1999). Moreover, they are also close to the spontaneous track measurements for RN and TI, suggesting that these apatites have also experienced at most limited heating over their geological histories.

4.3 Annealing models

Fitted parameters for the annealing models calculated for this study are shown in Table 4, and the index temperatures showing their geological time-scale predictions are listed in Table 5. The predicted annealing curves 23°C, representing a reasonable ambient temperature and adopted by convention from Donelick et al. (1990), are shown as solid lines in Figure 2. When considering these results, it is important to keep in mind that in addition to the low-temperature data shown there are varying amounts of high-temperature data (Table 4) that also influence the model fits and resulting 23°C predictions.

379 **Table 4**: Annealing models for individual apatites: Model parameters.

Apatite	N[1]	N[2]	N[3]	Length type	Fit	χ^2_ν	C_0	C_1	C_2	C_3	α	τ
DR	69	60	9	l_m	FC	1.54	-50.338	1.0255	-74.676	-8.1210	-0.8513	1.0594
					FA	1.46	-15.647	5.5043E-4	-16.178	7.5363E-4	-0.8984	1.0883
				l_c	FC	2.41	-54.628	1.1041	-105.28	-8.7728	-0.4104	1.0124
					FA	2.35	-15.132	5.0251E-4	-22.370	5.1659E-4	-0.3078	1.0124
FC	18	12	6	l_m	FC	0.58	-36.836	0.7574	-82.003	-8.3300	-1.0000	1.1072
					FA	0.42	-8.9095	3.03E-4	-14.500	7.77E-4	-1.0000	1.1616
				l_c	FC	0.52	-33.741	0.6379	-55.420	-7.7011	-1.0000	1.0856
					FA	0.58	-10.380	3.0835E-4	-11.992	9.1584E-4	-1.0000	1.1297
RN	63	55	8	l_m	FC	1.96	-80.451	1.7499	-102.12	-8.8076	-1.0000	1.0615
					FA	1.78	-22.018	8.5189E-4	-21.0071	5.1746E-4	-1.0000	1.0789
				l_c	FC	3.25	-23.320	0.4641	-37.2881	-7.3530	-0.3737	1.0166
					FA	3.00	-12.102	4.1411E-4	-13.9906	8.2108E-4	-0.3074	1.0166
TI	17	11	6	l_m	FC	1.35	-999.99	19.579	-2982.846	-65.0608	-1.0000	1.0845
					FA	1.27	-8.1882	2.5042E-4	-21.3969	6.1799E-4	-1.0000	1.1740
				l_c	FC	1.22	-997.96	19.866	-2072.036	-47.9494	-1.0000	1.0576
					FA	1.21	-22.185	6.8590E-4	-38.4459	4.9387E-6	-1.0000	1.0830

380 [1]Total number of data sets. [2]Number of high-T data sets from Carlson et al. (1999). [3]Number of low-T data sets from Tamer et al.
381 (2019) and this study
382

383 **Table 5**: Annealing models for individual apatite: predicted index temperatures and lengths.

Apatite	Data Sets	Length Type	Fit	$T_{F,100}$	$T_{F,30}$	$T_{F,10}$	$T_{C,1}$	$T_{C,10}$	$T_{C,100}$	$T_{A,1}$	$T_{A,10}$	$T_{A,100}$	$r_{Vrol,mean}$ [2]	r_{FC}
DR	High-T[1]	l_m	FC	83.1	92.1	100.4	89.2	107.2	126.4	102.5	120.4	139.1	-	-
			FA	117.5	124.1	130.3	121.5	135.4	150.3	133.5	146.9	161.3	-	-
		l_c*	FC	96.9	106.0	114.5	94.4	112.5	131.8	116.5	134.6	153.6	-	-
			FA	131.0	137.8	144.1	126.0	140.0	154.9	147.2	161.0	175.6	-	-
	Combined	l_m	FC	88.1	97.0	105.3	92.6	110.5	129.7	107.4	125.2	143.8	-	-
			FA	121.8	128.3	134.5	123.5	137.3	152.2	137.7	151.1	165.3	-	-
		l_c	FC	97.2	106.3	114.9	94.2	112.4	131.7	116.8	135.1	154.2	-	-
			FA	132.1	138.8	145.2	126.0	140.0	155.0	148.3	162.1	176.9	-	-
FC	High-T[1]	l_m	FC	113.7	123.0	131.7	109.6	128.1	147.8	133.6	152.1	171.5	-	0.9134
			FA	148.3	155.2	161.7	142.0	156.3	171.7	164.7	178.8	193.7	-	0.9522
		l_c	FC	121.9	131.1	139.7	112.9	131.2	150.8	141.6	159.9	179.1	-	0.9389
			FA	155.4	162.3	168.7	144.5	158.7	174.0	171.8	185.7	200.6	-	0.9658
	Combined	l_m	FC	105.6	115.0	123.7	105.4	124.1	143.9	125.5	144.3	163.9	-	0.9171
			FA	143.0	149.8	156.3	138.2	152.5	167.9	159.4	173.4	188.3	-	0.9460
		l_c	FC	121.2	130.3	138.8	113.6	131.6	150.7	140.7	158.8	177.7	-	0.9441
			FA	156.9	163.6	169.9	144.5	158.4	173.4	173.0	186.6	201.0	-	0.9626
RN	High-T[1]	l_m	FC	70.4	79.2	87.4	76.6	94.0	112.6	89.6	107.1	125.5	0.9101	-
			FA	104.8	111.3	117.3	108.4	121.9	136.4	120.6	133.7	147.8	0.9517	-
		l_c*	FC	85.1	94.1	102.6	79.5	97.1	115.9	104.6	122.6	141.5	0.9280	-
			FA	117.6	124.2	130.5	110.4	124.1	138.8	133.7	147.3	161.9	0.9650	-
	Combined	l_m	FC	65.2	74.1	82.4	72.2	89.9	108.9	84.5	102.4	121.2	0.8922	-
			FA	100.9	107.5	113.6	104.8	118.4	133.2	116.8	130.2	144.5	0.9433	-
		l_c	FC	88.2	97.1	105.3	81.3	98.5	117.0	107.4	125.0	143.5	0.9197	-
			FA	119.8	126.3	132.5	111.3	124.9	139.5	135.7	149.1	163.4	0.9596	-
TI	High-T[1]	l_m	FC	154.6	164.4	173.4	132.1	151.1	171.2	175.0	194.4	214.6	-	-
			FA	189.8	197.0	203.9	164.7	179.4	195.1	206.8	221.5	237.2	-	-
		l_c	FC	196.9	206.7	215.8	145.9	164.6	184.6	217.3	236.7	256.8	-	-
			FA	233.1	240.5	247.4	177.8	192.5	208.2	250.3	265.1	280.9	-	-
	Combined	l_m	FC	124.3	133.7	142.6	124.5	143.2	162.9	144.4	163.3	183.0	-	-
			FA	167.3	174.2	180.6	159.0	173.1	188.2	183.7	197.7	212.5	-	-
		l_c	FC	125.9	135.6	144.6	121.7	140.5	160.4	146.3	165.6	185.8	-	-
			FA	161.6	168.8	175.5	153.3	167.7	183.2	178.5	193.1	208.6	-	-

384 [1] High-T index temperatures from Ketcham et al. (1999), except asterisks indicate index temperatures from Ketcham et al. (2007). [2] Reduced
385 length for fluorapatite based on Vrolijk et al. (1992); target values 0.890-0.925 (non-projected), 0.925-0.950 (**c**-axis projected). [3] Reduced length
386 for FC apatite based on Ketcham et al. (2007); target values 0.937 ± 0.006 (non-projected), 0.959 ± 0.005 (**c**-axis projected).

The new models display a range of behaviors in comparison to the Ketcham et al. (1999) models. For DR apatite (Fig. 2a, b), the new model fits all of the low-temperature data well, with the exception of the shortest-time experiment. The fanning curvilinear fit also closely matches the spontaneous data, while the closure temperatures (Table 5) are only changed by 2-3°C, and other index temperatures by 4-7°C. Results are similarly congruent for FC apatite (Fig. 2c, d). Divergences are somewhat greater for the fanning Arrhenius models, and for the l_m versus the l_c models. These results suggest that the empirical fanning curvilinear fit to **c**-axis projected data is able to incorporate low-temperature, short-time data well, with a suitable change in the normalizing value. However, the normalizing values themselves show considerable variation, from 2.5% to 19.7% above the one-year-annealing l_0 measurements.

In contrast, the RN apatite models struggle to encompass the low-T data. This is in part due to the constraints imposed by the numerous high-temperature data, but it is also clear that neither model form or data type can encompass the low-T trend. Similarly, the TI models cannot fit the apparent two-component trend in our data, although, interestingly, they are consistent with, though offset from, the Donelick et al. (1990) data. In terms of index temperatures (Table 5), adding in the RN low-T data changes the results slightly more than for DR, although predicted closure temperatures still agree to within 4°C. The mismatch in TI index temperatures is greater, in part because the Ketcham et al. (1999) high-T models were fit in concert with all other apatites in Carlson et al. (1999), whereas here only TI data are being fitted. In particular, because the Carlson et al. (1999) TI data set includes no samples annealed to below a mean track length of 11.8 µm, the near-total-annealing behavior of this apatite is not well constrained.

Figure 3 shows the time residuals of mean **c**-axis projected length for each of the new models, distinguishing between high-temperature and low-temperature data. Standardized residuals (i.e. divided by uncertainty) are provided in the supplement and tell essentially the same story. Residuals from both linear and curvilinear models for the high-temperature data are flat to shallowly dipping; extending the linear fits to these residuals to geological time scales (~35 ln(s)) implies departures of 0.2 µm or less. Linear correlation coefficients are all less than 0.01. The larger DR and RN data sets show more scatter, but there is no readily apparent structure to any of the residuals. The low-T data, however, show significant structure, and in most cases are better fit by a logarithmic function than a line. The logarithmic fits imply a small positive residual of ~0.25 µm or less by 35 ln(s) for the four apatites.

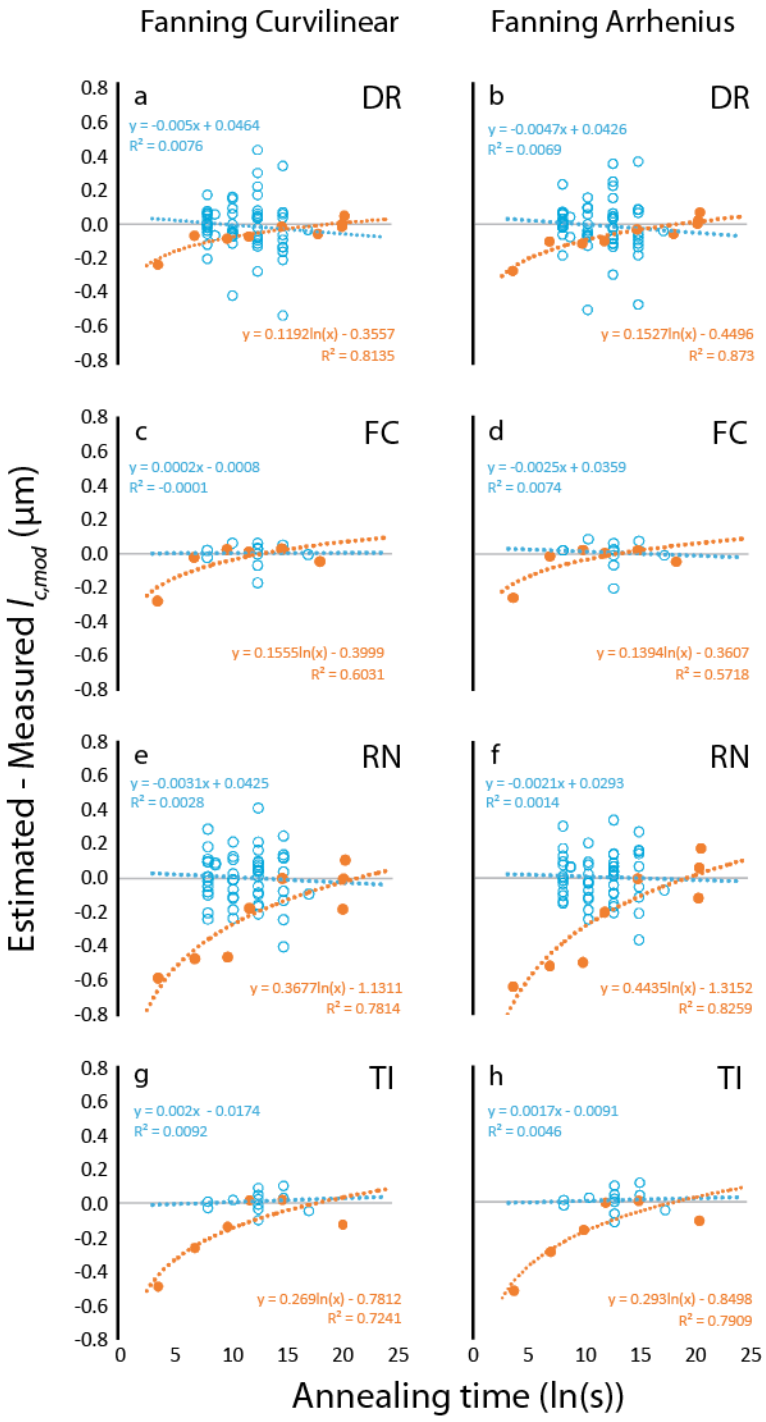

Figure 3: Time residuals of fitted model predictions for mean **c**-axis projected lengths for each apatite.

5 Discussion

5.1 Extending the range of annealing conditions

Apatite fission-track thermal history modelling is based on the extrapolation of annealing of induced tracks at laboratory conditions to geological time scales. Typically, model parameters are fitted by minimizing the misfit between model equation predictions and the data, and different model equations are evaluated and compared based on their degree of misfit and residuals (e.g., Laslett & Galbraith, 1996; Laslett et al., 1987), as well at their predictions against geological benchmarks (Ketcham et al., 1999). Because the various proposed empirical annealing equations overlap greatly over the limited time and temperature range of laboratory experiments (e.g., Ketcham, 2019, Fig. 3.9), extending this range provides a new opportunity to distinguish models by providing more space for them to diverge. Previous annealing studies covered temperature ranges of ~100°C to ~450°C and durations from ~30 minutes up to a couple of months, while this study extends annealing temperatures down to ~23°C and broadens the time range to span from 39 seconds to ~32 years (Figure 4).

In terms of goodness of fit, Ketcham et al. (1999) found that the fanning Arrhenius equation fit the Carlson et al. (1999) data slightly better than fanning curvilinear form, while Ketcham et al. (2007b) found that data from Barbarand et al. (2003) was sometimes better fit using the fanning curvilinear equation, depending on the form of *g* used. In this study (Table 4), we find that combined low-T and high-T DR and RN experimental data from Carlson et al. (1999) and this study were slightly better fit by the fanning Arrhenius form, while the TI and FC data were somewhat more closely fitted by the fanning curvilinear equation. Given that the DR and RN data sets show more extreme scatter (Fig. 3) and that χ^2_ν values are most sensitive to the most scattered points, we infer that the laboratory-time-scale data alone do not provide clear evidence of the superiority of one model form over the other, and that other considerations such as geological comparisons remain more informative.

While there is no discernible structure in the high-temperature residuals, the low-temperature data show a clear structure that diminishes with time. This suggests that there is a process occurring in the immediate aftermath of track formation that is not captured by either empirical annealing equation, but that this process may have a limited impact at longer laboratory or geological time scales.

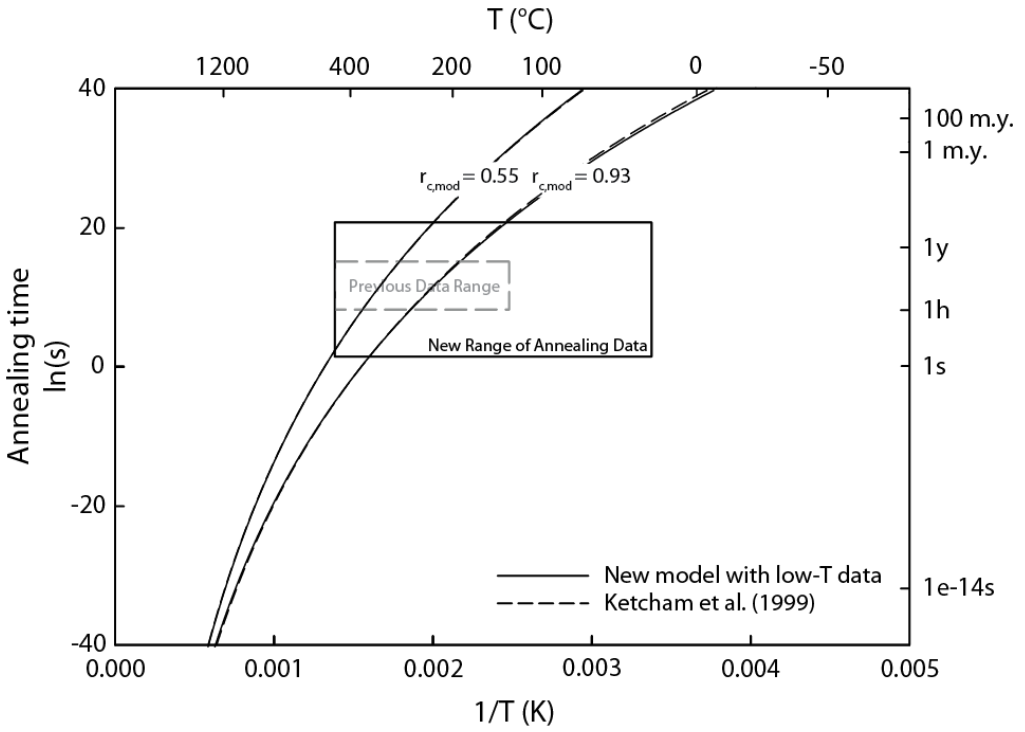

Figure 4: Illustration of extended range laboratory annealing data, and comparison of extrapolated predictions at low ($r_{c,mod}$ = 0.93) and high ($r_{c,mod}$ = 0.55) annealing conditions.

5.2 Geological predictions

Our fanning curvilinear fits for the DR and FC apatites both reproduce earlier work (Ketcham et al., 2007b; Ketcham et al., 1999) in making predictions that reasonably match their respective spontaneous track length data (Fig. 2a,b). As Figure 4 illustrates, the contours corresponding to reduced **c**-axis-projected length values for geological low-temperature (0.93) and total (0.55) annealing are not significantly impacted by incorporating the new data or making the true initial track length a fitted value. It is thus clear that incorporating the new low-temperature data did nothing to harm the geological predictions of these models based on apatites at both localities having resided at near-earth-surface temperatures since formation.

We also provide the first similar evaluation of Renfrew and Tioga apatites. Although the long-term burial histories at each locality are not known, both are likely to reflect long-term low-temperature histories. Renfrew, Ontario, is on the Canadian Shield, in an area of long-term stability. The apatite fission-track reference age for this locality is 184 ± 15 Ma (Van Den Haute & Chambaudet, 1990), while the U-Pb age of the enclosing pegmatite is ~1 Ga (Larsen et al., 1952). The Tioga apatite locality, near Old Port, Pennsylvania, is in the midst of the Valley and Ridge province. It is enclosed within the Marcellus Shale, and monazites in Tioga material collected nearby give a U-Pb age of 390 Ma (Roden et al., 1990). Tioga apatite from our sample's locality has a (U-Th)/He age of 280 Ma (Shuster et al., 2006), supporting long residence time at temperatures that probably remained below 60°C. While this area has undergone a complex history involving some burial, Tioga apatite has a substantially higher than normal resistance to annealing, and thus a greater ability to retain long track lengths with minor heating.

Our Renfrew fanning curvilinear model closely replicates our spontaneous track data assuming a mean track age of 92 Ma while residing at ~23°C. Our Tioga model predicts a slightly higher track length than observed assuming a mean age of 195 Ma at ~23°C, but if the residence temperature is raised to ~42°C the 15-µm mean **c**-axis-projected length is matched. These results, while rough and schematic, further support the idea that the fanning curvilinear model makes reasonable predictions of fission-track annealing in the near-surface environment. This in turn supports the validity of thermal history modeling results in the near-surface regime that utilize apatite fission-track length data.

5.3 Possibility of annealing due to secondary radiation

Our data strongly imply a second annealing mechanism in the initial stages, with different controlling equations or parameters. In particular, all four apatites show observable annealing in excess of the empirical model fits between the 39-second and 18-minute etching steps. A natural mechanism to consider is the secondary radiation produced by short-lived isotopes created during the irradiation. Other than induced fission of ^{235}U, several isotopes found in apatite in potentially significant quantities (^{19}F, ^{23}Na, ^{31}P, ^{35}Cl, ^{40,44}Ca, ^{55}Mn, ^{88}Sr, ^{139}La, ^{140}Ce, ^{146,148,150}Nd) interact with thermal neutrons through n,α and n,γ reactions to produce radioactive isotopes. Table S1 lists the unstable daughter products and their decay modes and half-lives, which range from seconds to months. The table also shows the estimated vacancies per decay caused by recoil, estimated using SRIM-2013 (Ziegler, 2013). We presume that only recoil damage is likely to affect track stability, and that emitted electrons and photons are not important; no significant activation products in apatite produce alpha particles. The only beta particle energetic enough to incur a recoil that results in any vacancies at all is ^{20}F produced from ^{19}F, and it averages 0.44 vacancies created per ion and has a stopping distance averaging 0.71 nm.

To scale the volume density of secondary recoils and the resulting damage to the fission damage zone, we normalize the density of decays and vacancies generated in Durango apatite at each stage of our experiment to the volume encompassed by a fission track. We estimate the latter as an ellipsoid with two short radii of 4.5 nm (Li et al., 2010) and one long radius of 9 µm. As of the end of the first etching step (39s), we find that there remain 6.2×10^{-5} activated ^{20}F atoms per track volume, which will have decayed by the second etching step, generating 2.75×10^{-5} vacancies per track volume. From these results, it is evident that recoil damage from activated isotopes is insufficient to have any effect on annealing rates.

5.4 Seasoning

Another candidate annealing mechanism is "seasoning," a vaguely defined process posited by several authors to explain track shortening at low temperatures (e.g., Durrani & Bull, 1987), possibly accompanied by a lack of apparent age reduction (Wauschkuhn et al., 2015). More generally, it can also serve as a placeholder for spontaneous tracks behaving differently from induced ones. Could the low-temperature annealing observed here correspond to seasoning, or at least one aspect of it?

At this stage, it is difficult to answer this question. Given that the effect we observe occurs at very short time scales, and seems to fade to insignificance at month-to-year time scales, much less millions-of-year ones, how it might apply to geological observations is unclear. One possibility is that it may be already broadly incorporated into the empirical fanning curvilinear

annealing equation. The curvature in the predicted annealing contours essentially posit more geological-time-scale annealing than the fanning linear forms that more closely reflect standard kinetics based on the Arrhenius equation. This curvature may be ascribable to temperature dependence in the kinetic frequency factor (Carlson, 1990; Ketcham, 2019), but superposition of multiple mechanisms may be a reasonable alternative. For example, molecular dynamics modeling suggests that there are multiple damage types and states within a track, ranging from slightly distorted lattice to amorphous or glassy material (Rabone et al., 2008), and different components of damage may anneal at different rates or by different mechanisms. Such variation may also underlie the different etching characteristics of spontaneous and induced fission tracks (Jonckheere et al., 2017).

A corollary question, posed in the title of this paper, is whether low-temperature annealing is a thermally controlled process. Certainly, insofar as much of our month-to-decade and geological data appear to be well described by the empirical equations, it is evident that most low-temperature annealing is indeed thermally controlled. However, with regard to an early-stage fast annealing process, our data are not sufficient to discern, if only because they only involve a single temperature; similar data at different temperatures may help address this question and elucidate details of the mechanism at work.

Yet another applicable question is how apatite composition may affect an early, low-temperature annealing process. The magnitude and rate of low-T annealing shows a fair degree of variation. In three of our four apatites (DR, FC, TI), annealing pathways essentially converge with the fanning curvilinear model within a month, while RN apatite is arguably still undergoing low-temperature annealing after 30 years, with double the net magnitude. The next most severe instance in terms of timing and departure from the fanning curvilinear model is TI. We are unable, however, to distinguish what features of these apatites may set them apart from the others. In both cation and anion compositions, RN and TI are the extremes of our apatites in terms of chemistry, and bracket DR and FC (Table 2). More data would thus be required to determine what features might influence the early, low-temperature process.

5.5 Reconsideration of mean unannealed track length

The data of our study indicate that mean "unannealed" track lengths decrease over seconds to years, with measured decreases of 0.74 μm for DR, 0.77 μm for FC, 1.49 μm for RN, and 0.81 μm for TI, with the majority of annealing occurring within the first month after irradiation. The cool-down waiting period after thermal neutron irradiation thus has a direct effect on the measured l_0, as well as any subsequent waiting time. Moreover, it is likely that the annealing of a fission track starts from the moment of its registration in the crystal lattice until it is etched. It is impossible to register and etch a fission track instantly and simultaneously, and therefore any track we observe is annealed to some degree.

Laslett and Galbraith (1996) proposed that the "true" unannealed length (μ_{max}), or at least the most appropriate value for normalizing measurements of annealed tracks, might be obtained by allowing it to be a free parameter when fitting an annealing model. However, their results, those of Ketcham et al. (2007b; 1999), and the results in this study suggest that this approach is not productive. Not only do the posited initial track lengths (μ_{max} or $\tau\ l_0$) vary much more widely than is reasonably suggested by the data themselves, but the possibility of an additional annealing mechanism responsible for the earliest stages of length reduction further muddies the picture. If the early-stage low-temperature annealing is not expressed in the high-temperature

annealing data, then using the high-temperature data to see back through early annealing cannot work.

At the same time, initial track length is important for incorporating differences both among apatites (Carlson et al., 1999) and among analysts (Ketcham et al., 2015; Ketcham et al., 2009; Ketcham et al., 2018) into the thermal history inverse modeling process. To the extent that thermal history results should be robust and reproducible, some method of normalization is required.

Based on our understanding of our results, we suggest that, when characterizing an unknown apatite, waiting through the fastest-declining part of the early annealing period is the safest method to measure an initial track length that will be consistent with literature values, and thus for comparison and usage across laboratories. Time after irradiation should be included when results are reported. Interested research groups may wish to make multiple grain mounts etched at various times after irradiation, to test or extend our results. Standardizing measurements to a particular time after irradiation may eventually be worthwhile, but because the low-temperature annealing process is poorly understood and likely of low magnitude after the first month, we do not yet consider such measures to be warranted.

6 Conclusions

Mean induced fission track lengths in apatite decrease from as early as 39 seconds after irradiation up to 32 years at room temperatures, with declines ranging from 0.7 to 1.5 µm. The rate of decrease can be separated into two behaviors, with faster shortening at early stages and slower shortening over longer periods at ambient temperatures that merges with trends predicted from empirical annealing equations. We thus posit the earlier behavior to reflect a mechanism not encompassed by the empirical equations. Although the rate, duration and magnitude of early-stage low-temperature annealing vary among the apatites we studied, we could not discern what chemical factors may control or influence this process. Fitted annealing models that combine high-T and low-T annealing better encompassed the low-T data but made similar geological time-scale predictions to models based on high-T data only. Comparison with spontaneous track data corroborates previous results indicating that the fanning curvilinear model form reasonably encompasses annealing at earth-surface temperatures. Additional experiments with more apatite varieties and/or at different temperatures may help us to discern more concerning the earlier annealing mechanism and further improve our knowledge of the annealing process.

Acknowledgments, Samples, and Data

This research was supported by the Jackson School of Geosciences at the University of Texas at Austin. It was also supported in part by National Science Foundation grant EAR-0948636 to RAK. We particularly thank Tracy Tipping of the Nuclear and Radiation Engineering Program and laboratory manager at the Nuclear Engineering Teaching Laboratory at the University of Texas at Austin for his help in planning and arranging for the experiment. We thank A. Gleadow for providing Renfrew apatite material for this study. We thank A. Gleadow, R. Jonckheere, and M. Cloos for helpful comments on an earlier version of this text. There are no financial conflicts of interest for either author. All measurements are available from the Texas Data Repository (https://doi.org/10.18738/T8/CUA8F8).

607

608 ## References

609

610

611 Barbarand, J., Carter, A., Wood, I., & Hurford, A. J. (2003). Compositional and structural control of fission-track
612 annealing in apatite. *Chemical Geology, 198*, 107-137. https://doi.org/10.1016/S0009-2541(02)00424-2
613 Belton, D. X. (2006). *The low-temperature thermochronology of cratonic terranes.* (PhD), University of Melbourne,
614 Retrieved from hdl.handle.net/11343/38119
615 Carlson, W. D. (1990). Mechanisms and kinetics of apatite fission-track annealing. *American Mineralogist, 75*,
616 1120-1139.
617 Carlson, W. D., Donelick, R. A., & Ketcham, R. A. (1999). Variability of apatite fission-track annealing kinetics I:
618 Experimental results. *American Mineralogist, 84*, 1213-1223. https://doi.org/10.2138/am-1999-0901
619 Crowley, K. D., Cameron, M., & Schaefer, R. L. (1991). Experimental studies of annealing etched fission tracks in
620 fluorapatite. *Geochimica et Cosmochimica Acta, 55*, 1449-1465. https://doi.org/10.1016/0016-
621 7037(91)90320-5
622 Donelick, R. A. (1991). Crystallographic orientation dependence of mean etchable fission track length in apatite: An
623 empirical model and experimental observations. *American Mineralogist, 76*(1-2), 83-91.
624 Donelick, R. A., Ketcham, R. A., & Carlson, W. D. (1999). Variability of apatite fission-track annealing kinetics II:
625 Crystallographic orientation effects. *American Mineralogist, 84*, 1224-1234. https://doi.org/10.2138/am-
626 1999-0902
627 Donelick, R. A., & Miller, D. S. (1991). Enhanced TINT fission track densities in low spontaneous track density
628 apatites using ^{252}Cf-derived fission fragment tracks: A model and experimental observations. *Nuclear*
629 *Tracks and Radiation Measurements, 18*(3), 301-307. https://doi.org/10.1016/1359-0189(91)90022-A
630 Donelick, R. A., O'Sullivan, P. B., & Ketcham, R. A. (2005). Apatite fission-track analysis. In P. W. Reiners & T.
631 A. Ehlers (Eds.), *Low-Temperature Thermochronology* (Vol. 58, pp. 49-94). Chantilly, VA: Mineralogical
632 Society of America. https://doi.org/10.2138/rmg.2005.58.3
633 Donelick, R. A., Roden, M. K., Mooers, J. D., Carpenter, B. S., & Miller, D. S. (1990). Etchable length reduction of
634 induced fission tracks in apatite at room temperature (~23°C): Crystallographic orientation effects and
635 "initial" mean lengths. *Nuclear Tracks and Radiation Measurements, 17*(3), 261-265.
636 https://doi.org/10.1016/1359-0189(90)90044-X
637 Durrani, S. A., & Bull, R. K. (1987). *Solid State Nuclear Track Detection* (Vol. 111). Oxford: Pergamon.
638 Fleischer, R. L., & Price, P. B. (1964). Techniques for geological dating of minerals by chemical etching of fission
639 fragment tracks. *Geochimica et Cosmochimica Acta, 28*(10-11), 1705-1714. https://doi.org/10.1016/0016-
640 7037(64)90017-1
641 Fleischer, R. L., Price, P. B., & Walker, J. D. (1965a). Effects of temperature, pressure, and ionization of the
642 formation and stability of fission tracks in minerals and glasses. *Journal of Geophysical Research, 70*(6),
643 1497-1502. https://doi.org/10.1029/JZ070i006p01497
644 Fleischer, R. L., Price, P. B., & Walker, R. M. (1965b). Tracks of charged particles in solids. *Science, 149*(3682),
645 383-393. https://www.jstor.org/stable/1716484
646 Fleischer, R. L., Price, P. B., Walker, R. M., & Maurette, M. (1967). Origins of fossil charged-particle tracks in
647 meteorites. *Journal of Geophysical Research, 72*(1), 331-353. https://doi.org/10.1029/JZ072i001p00331
648 Gleadow, A. J. W., & Duddy, I. R. (1981). A natural long-term track annealing experiment for apatite. *Nuclear*
649 *Tracks and Radiation Measurements, 5*, 169-174. https://doi.org/10.1016/0191-278X(81)90039-1
650 Gleadow, A. J. W., Duddy, I. R., Green, P. F., & Lovering, J. F. (1986). Confined fission track lengths in apatite: a
651 diagnoastic tool for thermal history analysis. *Contributions to Mineralogy and Petrology, 94*, 405-415.
652 https://doi.org/10.1007/BF00376334
653 Gleadow, A. J. W., Harrison, T. M., Kohn, B. L., Lugo-Zazueta, R., & Phillips, D. (2015). The Fish Canyon Tuff: A
654 new look at an old low-temperature thermochronology standard. *Earth and Planetary Science Letters, 424*,
655 95-108. https://doi.org/10.1016/j.epsl.2015.05.003
656 Green, P. F. (1988). The relationship between track shortening and fission track age reduction in apatite: Combined
657 influences of inherent instability, annealing anisotropy, length bias and system calibration. *Earth and*
658 *Planetary Science Letters, 89*, 335-352. https://doi.org/10.1016/0012-821X(88)90121-5
659 Issler, D. R. (1996). Optimizing time step size for apatite fission track annealing models. *Computers and*
660 *Geosciences, 22*, 67-74. https://doi.org/10.1016/0098-3004(95)00057-7

Jonckheere, R. (2003). On methodical problems in estimating geological temperature and time from measurements of fission tracks in apatite. *Radiation Measurements, 36*, 43-55. https://doi.org/10.1016/S1350-4487(03)00096-9

Jonckheere, R., Tamer, M. T., Wauschkuhn, B., Wauschkuhn, F., & Ratschbacher, L. (2017). Single-track length measurements of step-etched fission tracks in Durango apatite: "Vorsprung durch Technik". *American Mineralogist, 102*(5). https://doi.org/10.2138/am-2017-5988

Ketcham, R. A. (2003). Observations on the relationship between crystallographic orientation and biasing in apatite fission-track measurements. *American Mineralogist, 88*, 817-829. https://doi.org/10.2138/am-2003-5-610

Ketcham, R. A. (2019). Fission-track annealing: From geologic observations to thermal history modeling. In M. G. Malusà & P. G. Fitzgerald (Eds.), *Fission-Track Thermochronology and its Application to Geology*. Cham: Springer. https://doi.org/10.1007/978-3-319-89421-8_3

Ketcham, R. A., Carter, A., & Hurford, A. J. (2015). Inter-laboratory comparison of fission track confined length and etch figure measurements in apatite. *American Mineralogist, 100*, 1452-1468. https://doi.org/10.2138/am-2015-5167

Ketcham, R. A., Carter, A. C., Donelick, R. A., Barbarand, J., & Hurford, A. J. (2007a). Improved measurement of fission-track annealing in apatite using c-axis projection. *American Mineralogist, 92*, 789-798. https://doi.org/10.2138/am.2007.2280

Ketcham, R. A., Carter, A. C., Donelick, R. A., Barbarand, J., & Hurford, A. J. (2007b). Improved modeling of fission-track annealing in apatite. *American Mineralogist, 92*, 799-810. https://doi.org/10.2138/am.2007.2281

Ketcham, R. A., Donelick, R. A., Balestrieri, M. L., & Zattin, M. (2009). Reproducibility of apatite fission-track length data and thermal history reconstruction. *Earth and Planetary Science Letters, 284*, 504-515. https://doi.org/10.1016/j.epsl.2009.05.015

Ketcham, R. A., Donelick, R. A., & Carlson, W. D. (1999). Variability of apatite fission-track annealing kinetics III: Extrapolation to geological time scales. *American Mineralogist, 84*, 1235-1255. https://doi.org/10.2138/am-1999-0903

Ketcham, R. A., Van Der Beek, P. A., Barbarand, J., Bernet, M., & Gautheron, C. (2018). Reproducibility of thermal history reconstruction from apatite fission-track and (U-Th)/He data. *Geochemistry, Geophysics, Geosystems, 19*. https://doi.org/10.1029/2018GC007555

Larsen, E. S. J., Keevil, N. B., & Harrison, H. C. (1952). Method for determining the age of igneous rocks using the accessory minerals. *Geological Society of America Bulletin, 63*, 1046-1052. https://doi.org/10.1130/0016-7606(1952)63[1045:MFDTAO]2.0.CO;2

Laslett, G. M., & Galbraith, R. F. (1996). Statistical modelling of thermal annealing of fission tracks in apatite. *Geochimica et Cosmochimica Acta, 60*, 5117-5131. https://doi.org/10.1016/S0016-7037(96)00307-9

Laslett, G. M., Green, P. F., Duddy, I. R., & Gleadow, A. J. W. (1987). Thermal annealing of fission tracks in apatite 2. A quantitative analysis. *Chemical Geology (Isotope Geoscience Section), 65*, 1-13. https://doi.org/10.1016/0168-9622(87)90057-1

Li, N., Wang, L., Sun, K., Lang, M., Trautmann, C., & Ewing, R. C. (2010). Porous fission fragment tracks in fluorapatite. *Physical Review B, 82*, 144109. https://doi.org/10.1103/PhysRevB.82.144109

McDowell, F. W., McIntosh, W. C., & Farley, K. A. (2005). A precise ^{40}Ar-^{39}Ar reference age for Durango apatite (U-Th)/He and fission-track dating standard. *Chemical Geology, 214*, 249-263. https://doi.org/10.1016/j.chemgeo.2004.10.002

Meitner, L., & Frisch, O. R. (1939). Disintegration of uranium by neutrons: a new type of nuclear reaction. *Nature, 143*(3615), 239-240. https://doi.org/10.1038/143239a0

Naeser, C. W. (1967). The use of apatite and sphene for fission track age determinations. *Geological Society of America Bulletin, 78*(12), 1523-1526. https://doi.org/10.1130/0016-7606(1967)78[1523:TUOAAS]2.0.CO;2

Naeser, C. W., Zimmerman, R. A., & Cebula, G. T. (1981). Fission-track dating of apatite and zircon: An interlaboratory comparison. *Nuclear Tracks and Radiation Measurements, 5*, 56-72. https://doi.org/10.1016/0191-278X(81)90027-5

Price, P. B., & Walker, R. M. (1963). Fossil tracks of charged particles in mica and the age of minerals. *Journal of Geophysical Research, 68*(16), 4847-4862. https://doi.org/10.1029/JZ068i016p04847

Rabone, J. A. L., Carter, A., Hurford, A. J., & De Leeuw, N. H. (2008). Modelling the formation of fission tracks in apatite minerals using molecular dynamics simulations. *Physics and Chemistry of Minerals, 35*, 583-596. https://doi.org/10.1007/s00269-008-0250-6

Roden, M. K., Parrish, R. R., & Miller, D. S. (1990). The absolute age of the Eifelian Tioga ash bed, Pennsylvania. *Journal of Geology*, *98*(2), 282-285. www.jstor.org/stable/30063775 https://doi.org/10.1086/629399

Shuster, D. L., Flowers, R. M., & Farley, K. A. (2006). The influence of natural radiation damage on helium diffusion kinetics in apatite. *Earth and Planetary Science Letters*, *249*, 148-161. https://doi.org/10.1016/j.epsl.2006.07.028

Silk, E. C. H., & Barnes, R. S. (1959). Examination of fission fragment tracks with an electron microscope. *Philosophical Magazine*, *4*(44), 970-972. https://doi.org/10.1080/14786435908238273

Spiegel, C., Kohn, B. L., Raza, A., Rainer, T., & Gleadow, A. J. W. (2007). The effect of long-term low-temperature exposure on apatite fission track stability: A natural annealing experiment in the deep ocean. *Geochimica et Cosmochimica Acta*, *71*, 4512-4537. https://doi.org/10.1016/j.gca.2007.06.060

Tamer, M. T., Chung, L., Ketcham, R. A., & Gleadow, A. J. W. (2019). Analyst and etching protocol effects on the reproducibility of apatite confined fission-track length measurement, and ambient-temperature annealing at decadal timescales. *American Mineralogist*, *104*, 1421-1435. https://doi.org/10.2138/am-2019-7046

Van Den Haute, P., & Chambaudet, A. (1990). Results of an interlaboratory experiment for the 1988 fission track workshop on a putative apatite standard for internal calibration. *International journal of radiation applications and instrumentation. Part D, Nuclear tracks and radiation measurements*, *17*(3), 247-252. https://doi.org/10.1016/1359-0189(90)90042-V

Vrolijk, P., Donelick, R. A., Queng, J., & Cloos, M. (1992). Testing models of fission track annealing in apatite in a simple thermal setting: site 800, leg 129. In R. L. Larson & Y. Lancelot (Eds.), *Proceedings of the Ocean Drilling Program, Scientific Results* (Vol. 129, pp. 169-176). College Station, TX: Ocean Drilling Program.

Wagner, G. A. (1968). Fission track dating of apatites. *Earth and Planetary Science Letters*, *4*(5), 411-415. https://doi.org/10.1016/0012-821X(68)90072-1

Wauschkuhn, B., Jonckheere, R., & Ratschbacher, L. (2015). The KTB apatite fission-track profiles: Building on a firm foundation? *Geochimica et Cosmochimica Acta*, *167*, 27-62. https://doi.org/j.gca.2015.06.015

Ziegler, J. F. (2013). SRIM-2013 The stopping and range of ions in matter. Annapolis: United States Naval Academy. Retrieved from http://www.srim.org/